RASĀYAN *J. Chem.*
Vol. 17 | No. 1 |95-104| January - March | 2024
ISSN: 0974-1496 | e-ISSN: 0976-0083 | CODEN: RJCABP
http://www.rasayanjournal.com
http://www.rasayanjournal.co.in

AMORPHOUS SILICA MICROSPHERE FROM OPENLY BURNED RICE HUSK ASH AS AN EFFICIENT ADSORBENT FOR ULTRASOUND-ASSISTED METHYLENE BLUE REMOVAL

Q. Lailiyah[1], N. T. E. Darmayanti[1], M.R. Mulyana[1], N. Nuryatini[1], A. Hapiddin[1], B. Basuki[1], O. Zuas[1,✉], S. A. Rahmah[2], A. N. Fadhila[2], N. Aryana[3], H. H. Kurniawan[3], A. Andreas[3], W. K. Restu[3], F. Aulia[3], T. Sudiro[4] and D. Nanto[5]

[1]Research Centre for Testing Technology and Standard, BRIN, KST BJ Habibie, Tangerang Selatan, 15314, Indonesia
[2]Department of Chemistry, FMIPA, Universitas Indonesia, Depok, 1640, West Java, Indonesia
[3]Research Centre for Chemistry, BRIN, KST BJ Habibie, Tangerang Selatan, 15314, Indonesia
[4]Research Centre for Advance Material, BRIN, KST BJ Habibie, Tangerang Selatan, 15314, Indonesia
[5]Departement of Physic Education, UIN Syarif Hidayatullah, Tangerang Selatan, 15412, Indonesia
✉Corresponding Author: oman003@brin.go.id

ABSTRACT

In this study, silica (SiO_2) was fabricated from a sodium silicate solution derived from an openly burned rice husk using precipitation followed by calcining at 500 ºC for five hours. The calcined SiO_2 was well-characterized using TGA, XRD, Raman spectroscopy, Nitrogen adsorption-desorption, FTIR, XRF, and FESEM. The results showed that the calcined SiO_2 has an amorphous phase, spherical particle shape with micrometer-sized, and belongs to mesoporous material. The fabricated SiO_2 was evaluated as an adsorbent for methylene blue removal from an aqueous solution using the ultrasound-assisted adsorption technique. The adsorption parameters including pH of the solution, the dosage of the adsorbent, initial concentration of dye in solution, and adsorption time were evaluated. They revealed the optimum values of 10, 2.5 g/L, 20 ppm, and 10 min, respectively. Under this optimum condition, the adsorption efficiency was found to be 98.43%. The findings implied that the fabrication of SiO_2 from openly burned rice husk using a precipitation method is facile and the fabricated SiO_2 could be a prospective adsorbent for removing industrial dye waste effluents.

Keywords: Silica, Amorphous, Rice Husk, Adsorbent, Methylene Blue, Ultrasound.

RASĀYAN *J. Chem.*, Vol. 17, No.1, 2024

INTRODUCTION

The utilization of rice husk (RH) as an alternative raw material for manufacturing silica (SiO_2) in the creation of functional materials is a promising recycling method. The RH combustion process under controlled temperatures[1, 2] and the basic chemical digestion processes[3, 4] are low-cost methods for obtaining SiO_2 from RH. These efforts are expected to contribute to the sustainable waste management of RH. The RH-generated SiO_2 has unique properties and has been extensively investigated for many purposes, such as addressing environmental pollution issues,[5] medical and biotechnology,[6] energy,[7] construction materials,[8] and agriculture.[9] In the area of environmental remediation, fabrication methods and benefits of the RH-generated SiO_2 as an adsorbent for treating dye pollutants have been previously reported.[5, 10-14] Tolba *et al*.[14] demonstrated that a high-efficiency methylene blue (MB) removal can be achieved by using nano-sized SiO2 particles derived from RH extracted using hydrothermal methods. Nguyen *et al*.[11] and Thu *et al*.[13] have successfully extracted mesoporous SiO_2 from RH using cetyltrimethylammonium bromide (CTAB) as a surfactant for MB removal from the solution. Peres *et al*.[12] used microwave technology to extract SiO_2 nanoparticles from RH and obtained an effective adsorbent in removing MB from the solution.

http://doi.org/10.31788/RJC.2024.1718726

Villota-Enríquez and Rodríguez-Páez[5] and Haider *et al*.[10] recently reported that high-efficiency adsorbents for removing MB from solution were obtained from openly burned rice husk ash (OB-RHA) and RH, respectively. Still, as far as is known, the study on the preparation of micro-sized amorphous SiO_2 from OB-RHA with spherical particles and its usage as an adsorbent for MB dye removal utilizing an ultrasound-assisted technique has not been reported. This study aimed to fabricate micro-sized amorphous SiO_2 by a simple digestive method in the presence of methanol using OB-RHA as the silicon source. The fabricated SiO_2 was characterized using TGA, XRD, Raman spectroscopy, Nitrogen adsorption-desorption, FTIR, XRF, and FESEM, while its adsorption power was evaluated for MB dye removal from solution.

EXPERIMENTAL

Materials and Methods

The OB-RHA (Fig.-1a) was gifted by a paddy rice processing mill company in Banjarsari Wonosobo, Tanggamus, Lampung, Indonesia. Sulfuric acid (H_2SO_4, 95-97% purity), hydrochloric acid (HCl, 32% purity), and methanol (CH_3OH, ≥ 99.9% purity) were obtained from Merck, Darmstadt, Germany. Sodium hydroxide (NaOH, 99% purity) was acquired from Sigma Aldrich, Darmstadt, Germany. Methylene blue (MB, C.I. 52015) was bought from Merck, Darmstadt, Germany. All these chemicals were directly used without any treatment. All experimental runs used ultra-pure water from the direct purification system (Milli-Q, Merck Millipore, MA, USA). The instruments used for the characterization are a Thermogravimetric Analyzer (TGA STA PT 1600 Linseis Messgeraete, Selb, Germany), X-ray diffractometer (XRD D8 Advanced Rigaku SmartLab, Tokyo, Japan), Fourier Transform Infrared Spectrometer (FT-IR, Bruker Tensor II, MA, USA), BET analyzer (Tristar II, Micromeritics Instrument Corporation, USA), X-ray Fluorescence Spectrometer (XRF, Bruker S2 Puma, MA, USA), Raman Spectrometer (RAMAN, Horiba Scientific, Kyoto, Japan), Field Emission-Scanning Electron Microscope (JIB-4610F, Jeol, Tokyo, Japan), Particle Size Analyzer (PSA, NanoPlus, Particulate Systems, Georgia, USA).

Fabrication of SiO_2 from OB-RHA

The amorphous SiO_2 microsphere was fabricated using a procedure adopted from the literature with modification.[10,15] Typically, the OB-RHA sample (Fig.-1a) was acid-treated to remove unwanted material and surface impurities followed by washing twice with tap water before being dried at 105 ºC for 24 h. The dried OB-RHA was crushed and sieved through a 140 mesh (~105 μm) sieve. After that, the water-treated and sieved OB-RHA (20 g) was transferred into a reflux flask containing 200 ml HCl solution (1.5 mol/L). The reflux process was conducted under heating at 65 ºC and constant stirring for two hours. The suspension was separated by Whatman grade 1 ashless filter paper. The solid residues were then collected and washed with ultra-high purity water until they reached a neutral pH, followed by heating at 120 ºC for 24 hours. A highly alkaline sodium silicate (Na_2SiO_3), as the SiO_2 precursor, was obtained from acid-treated OB-RHA (Fig.-1b). In a typical procedure, the acid-treated OB-RHA (10 g) was placed in a 250 mL polypropylene beaker containing an alkaline solution (NaOH 200 mL, 2.5 M), followed by heating at 80 ºC under constant stirring for two hours. The solid residues were discarded from Na_2SiO_3 suspension by filtering using Whatman grade 41 ashless filter paper. The SiO_2 was extracted from the prepared Na_2SiO_3 solution (Fig.-1c) using the following procedure. The highly alkaline Na_2SiO_3 (20 mL) and methanol (7.5 mL) were initially transferred into a 100 mL beaker and well-mixed. The mixture was then precipitated with a 2 M H_2SO_4, and gel formation began when the pH fell below 10. The precipitation process was kept until pH 7 under constant stirring to avoid changes in local pH during gel formation. The gel formed was stirred for 15 min and then collected followed by washing with water until a constant pH. The gel was dried overnight at 80 ºC and labelled as-prepared OB-RHA SiO_2. Finally, the as-prepared OB-RHA SiO_2 (Fig.-1d) was calcined for five hours at 500 ºC. The calcined OB-RHA SiO_2 (Fig.-1e) was kept for further characterization and adsorption activity evaluation.

Dye Adsorption Tests

The ultrasound-assisted adsorption (UAA) evaluation was conducted using a batch test in an ultrasonic apparatus (Branson Bransonic®, Mechanical Bath 8800, Emerson, USA). A known concentration of MB solution was transferred into a 50 mL vial, followed by adding a fixed amount of calcined OB-RHA SiO_2

as adsorbent. The mixture-containing vial was placed in an ultrasonic apparatus chamber, and the adsorption experiment began. After a predetermined adsorption time, a specific amount of MB solution was taken. The adsorbent was discarded from the treated solution using a centrifuge at 6,000 rpm for 5 mins. A scanning UV-vis spectrophotometer was employed to measure the absorbance of the treated solution within the range of 200-800 nm. To determine the residual MB concentration in the treated solution, the absorbance of the treated solution was inserted into a calibration curve ($Y = 0.1593X + 0.036$, $R^2 = 0.999$) derived from a series of MB standard solutions ranging from 0 to 40 ppm. The adsorption efficiency (%) of the calcined OB-RHA SiO_2 in removing MB was calculated using Eq.-1.[16]

$$\text{Adsorption efficiency (\%)} = {C_o - C_t}/{C_o} \times 100 \quad (1)$$

where C_o is MB concentration (ppm) at $t = 0$ min, and C_t is MB concentration (ppm) at $t = t$ min.

RESULTS AND DISCUSSION

Fabrication of SiO_2

In SiO_2 fabrication, any element other than SiO_2 itself is considered an impurity[17] and must be reduced to the greatest extent if it cannot be completely removed. Reducing impurities was done by treating the OB-RHA in an acid solution and then drying it at a moderate temperature. The powdered OB-RHA (Fig.-1b) obtained from acid treatment was leached using an alkaline solution to generate a Na_2SiO_3 solution with a yellowish appearance (Fig.-1c). The leaching process follows a chemical reaction,[10] as shown in Eq.-2. Moreover, because the Na_2SiO_3 solution is alkaline, SiO_2 can be extracted easily using the acid precipitation method[10,15] and the chemical reaction may follow Eq.-3.[10] Separation and evaporation techniques were used to obtain the as-prepared OB-RHA SiO_2 (Fig.-1d). The as-prepared OB-RHA SiO_2 (Fig.-1e) was obtained by the calcination at 500 ºC for five hours.

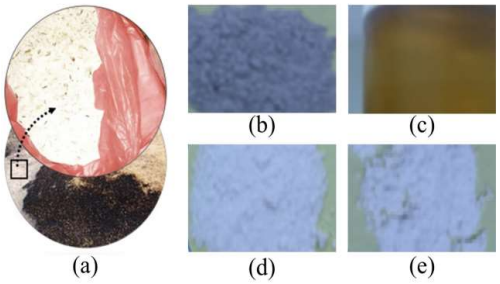

Fig.-1: (a) Openly Burned Rice Husk Ash (OB-RHA), (b) Acid-Treated OB-RHA, (c) Sodium Silicate Solution with a Clear and Yellowish Appearance, (d) as-prepared OB-RHA SiO_2 Powder, and (e) Calcined OB-RHA SiO_2

$$\text{OB-RHA-}SiO_{2\,(solid)} + 2NaOH_{(liquid)} \rightarrow Na_2SiO_{3(liquid)} + H_2O_{(liquid)} \quad (2)$$

$$Na_2SiO_{3(liquid)} + H_2SO_{4(liquid)} \rightarrow \text{OB-RHA } SiO_{2(solid)} + Na_2SO_{4(liquid)} + H_2O_{(liquid)} \quad (3)$$

Characterizations

Figure-2a depicts the thermogram of as-prepared OB-RHA SiO_2 measured at 25 to 800 ºC. The TGA analysis predicts ~27.9% weight loss due to mass decomposition in two stages. The first mass loss (~21.3%) due to the loss of water moisture from the SiO_2 surface[18] at temperatures below 200 ºC. The second mass loss (~7.6%) occurred at temperatures in the range of 200-800 ºC, corresponding to the formation of Si-O-Si (siloxane) from the Si-OH (silanol) group.[18,19] The XRD spectrum of calcined OB-RHA SiO_2 is shown in Fig.-2b. A hump at 2θ between 15-30º with a centered peak value at 2θ = 21.9º indicates the formation of amorphous SiO_2 (JCPDS-card # 96- 412-4080).[20] This 2θ centered value is close to the centered peak values reported in previous studies.[4, 10, 12, 21] Azat *et al.*[21] reported that 600 ºC of calcination temperature led to the formation of an amorphous SiO_2 with 2θ = 22º, El-Sakhawy *et al.*[4] found that an amorphous SiO_2 with 2θ = 22.5º was obtained at 550 ºC of calcination temperature. Haider *et al.*[10] observed that an amorphous SiO_2 with 2θ = 21.7º can be obtained without calcination. Peres *et al.*[12] stated that the formation of amorphous SiO_2 with 2θ = 22º was generated at a calcination temperature of 700 ºC. These 2θ data indicate that elevating the calcination temperature may induce the central peak of amorphous SiO_2 to shift

towards a lower value.[10] In addition, no 2θ peaks belonging to crystalline SiO_2 could be observed in Fig.-2b, indicating that the calcined OB-RHA SiO_2 is in a pure amorphous phase. Instead, the phase transformation of SiO_2 from amorph to crystalline would occur commonly at higher calcination temperatures (>800 °C).[15]

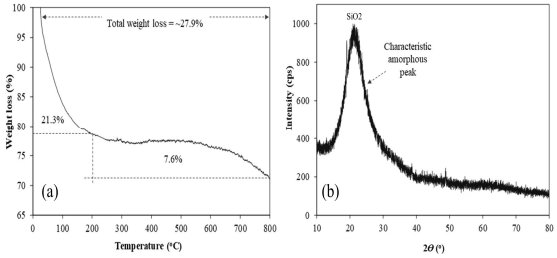

Fig.-2: (a) Thermogram of as-prepared OB-RHA SiO_2 and (b) XRD Pattern of Calcined OB-RHA SiO_2

Figure-3a displays the measured FTIR spectrum of calcined OB-RHA SiO_2. This spectrum shows two firm absorption peaks at around 799.14 cm^{-1} and 1076.5 cm^{-1}, which are linked to the asymmetric stretching vibration of Si-O-amorphous SiO_2 and Si-O-Si compounds, respectively.[22] These two firm absorption peaks are very close to the values of amorphous SiO_2 reported by Santana Costa *et al*.,[15] and Haider *et al.*[10] Their strong peak might be attributed to completely removing any possible impurities during calcination. The existence of bending absorption and vibration mode of the H_2O molecules on the surface of SiO_2,[3,18] which are indicated by very weak absorption bands at around 1634 cm^{-1} and around 3438 cm^{-1}, respectively, are also observed in Fig.-3a. Figure-3b shows the vibrational Raman modes of SiO_2 which is generally indicated by a spectrum at a band below 1200 cm^{-1}.[23] As shown in Fig.-3b, vibrational bands below 1200 cm^{-1} exist in a broad spectrum, characteristic of SiO_2 as an amorphous phase. This broad spectrum is caused by the irregular bond angles and bond length arrangement in amorphous SiO_2.[24, 25] Two bands in the frequency region between 400 cm^{-1} and 700 cm^{-1} are related to the inter-tetrahedral Si-O-Si bonding.[26] Meanwhile, the bands from 700 cm^{-1} to 1100 cm^{-1} frequency region correspond to the Si-O- stretching vibrations in tetrahedrons of different silicates.[27] The amorphous SiO_2 bands have low intensity. However, additional bands of other element impurities in the SiO_2 sample may affect the band intensity. Band with low intensity, around 451 cm^{-1}, is a signal generated by O-Si-O bending vibration. Two other low-intensity bands in the 490 - 610 cm^{-1} range correspond to the three or four siloxane rings or are associated with the structural defects due to bond damage in the SiO_2 network.[28] A band around 802 cm^{-1} corresponds to a symmetrical Si-O-Si stretching vibration.[29,30] This broad and high intensity is likely due to superimposed by bending vibration signals of P_2O_5 bonds and active vibrations of bulk Al_2O_3 bonds at regions 708 - 794 cm^{-1} and region 748 cm^{-1},[29, 31] respectively. A band at 920 cm^{-1} is a band characteristic of tetrahedral silicate and its vigorous intensity due to superimposed by the PO_4 functional peak at 958 cm^{-1}. Meanwhile, the band observed at 980 cm-1 relates to the stretching vibrations of Si-O- units. Non-symmetric Si-O-Si stretching vibration is visible at a band around 1003 cm^{-1}.[30] Two other bands, around 1050 cm^{-1} and around 1200 cm^{-1}, are associated with the symmetrical stretching of silicon and oxygen in the tetrahedral silicate, which has non-bridging oxygen atoms,[26] respectively. The adsorption isotherm of calcined OB-RHA SiO_2 is depicted in Fig.-3c. The adsorption-desorption behavior within the mesopore structure due to capillary condensation, also known as loop hysteresis, was observed in the P/Po range between 0.8 and 1.0. According to the IUPAC classification,[32] the calcined OB-RHA SiO_2 has a type IV adsorption isotherm with a type H3 hysteresis ring. BET analysis found that the calcined OB-RHA SiO_2 has a specific surface area of 19.33 m^2/g, an average pore size of 0.071 cm^3/g, and a diameter pore average of 14.75 nm. From the inset of Fig.-3c, the OB-RHA SiO_2 has a sharp pore width in the 2.05 to 21.72 nm range, classifying calcined OB-RHA SiO_2 as a mesopore material.[18,32] The BET surface area of the calcined OB-RHA SiO_2 is much lower than the surface area of amorphous SiO_2 from rice-based biomass found in the literature.[10,33] The variation in the BET-specific surface area values could be due to differences in treatment methods or caused by some residual components in SiO_2 derived from the chemicals used during preparation. Haider *et al*.,[10] and Fernandes *et al*.,[33] showed that different extraction treatments affect the specific surface area of the SiO_2 obtained. While Park *et al*.,[34] reported that the Na_2O originating from NaOH leaching may affect the surface melting and agglomeration, leading to a reduced surface area of SiO_2 obtained. According to the XRF

composition analysis, the yield of calcined OB-RHA SiO_2 obtained is 94.20 %, which is comparable to the purity level of extracted SiO_2 from rice-based biomass as reported by previous researchers.[3,10] Some other elements commonly found in biomass were also detected, including Na_2O (1.80%), MgO (1.50%), Al_2O_3 (1.10%), SO_3 (0.90%), P_2O_5 (0.40%), and CaO (0.10%). The amount and composition of these elements highly depend on the soil characteristics, harvest year, and the type of fertilizer used, which may differ from one location to another.[15,33] The Na_2O is the second highest element detected, whose presence may originate either from rice-growing soil,[10,24] or from incomplete removal of NaOH solution used in the extraction process.[10,34] SO_3 most likely originated from trapped and un-leached ions in the sample, and Al_2O_3 might be derived from rice-growing soil. According to Dell *et al.*, as cited in Santa Costa *et al*.,[15] , residual CaO and MgO may come from soil reservoirs. At the same time, P_2O_5 is associated with the type of fertilizers used in rice cultivation.

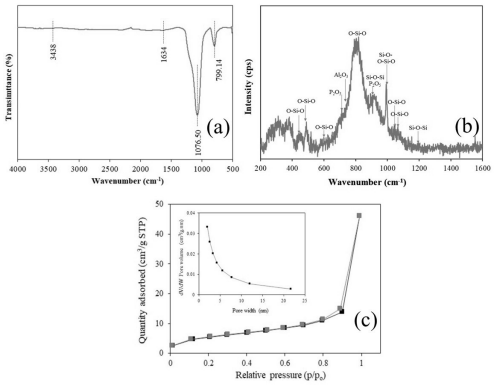

Fig.-3: (a) FTIR Spectrum, (b) Raman Spectrum, and (c) N_2 Adsorption−Desorption Isotherms (Insert: pore size distributions) of Calcined OB-RHA SiO_2

Figure-4 shows FESEM micrographs of calcined OB-RHA SiO_2 and their monomodal particle size distribution curves. The images in Fig.-4a-c display the surface texture and morphology of calcined OB-RHA SiO_2, which is mostly sphered in particle shapes that vary in size and have a hard agglomeration appearance. The formation of such spherical particle shape could be attributed to the incorporation of methanol, which may have impeded the rates of condensation and hydrolysis during precipitation.[35] DLS analysis (Fig.-4d) reveals that calcined OB-RHA SiO_2 has particle sizes ranging from 0.35 to 1.67 micrometers.

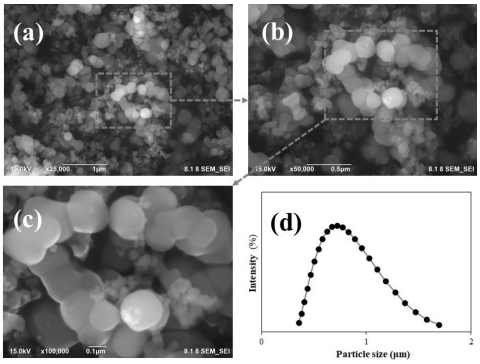

Fig.-4: (a-c) Typical Morphology Images of Calcined OB-RHA SiO_2 with Different Magnifications and (d) its DLS Size Distribution

Figures-5a, -5b, and -5c-j show an EDS scan area, EDS spectrum, and EDS elemental distribution mapping of calcined OB-RHA SiO_2, respectively. The EDS scan area (Fig.-5a) was taken at the same region as in Fig.-4b. The EDS spectrum in Fig.-5b clearly shows the elements in the calcined OB-RHA SiO_2 sample. Two peaks with strong intensities belong to Si and O elements, confirming that SiO_2 is the predominant element in calcined OB-RHA SiO_2. The presence of other elements, including Ca, Na, Mg, Al, S, and P, also can be observed in Fig.-5b with very weak intensity. This finding agrees with the result of Raman

spectroscopy and XRF analysis. Moreover, Fig.-5c-j depicts the EDS mapping, displaying the distribution location of element on the SiO_2 surface.

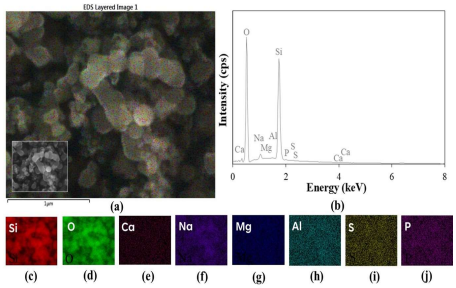

Fig.-5: EDS Data of Calcined OB-RHA SiO_2: (a) an EDS SCAN AREA, (b) EDS Spectrum, and EDS Mapping Results of (c) Si-, (d) O-, (e) Ca-, (f) Na-, (g) Mg-, (h) Al-, (i) S-, and (j) P-Element Distribution

Adsorption Activity Evaluation

A comparison of the adsorption efficiencies of the UAA and conventional agitation adsorption (CAA) methods was performed. As shown in Fig.-6a, the UAA resulted in a higher adsorption efficiency (98.82%) than the CAA method (73.11%), and the MB spectra resulted are depicted in Fig.-6b. The enhanced adsorption efficiency observed with the UUA method can be ascribed to an increment in mass transfer at the interfaces between liquids and solids. This occurs via translational motion induced by acoustic cavitation, which encompasses the processes of bubble formation, expansion, and collapse.[36] Acoustic cavitation may also create pore structures on the surface of the adsorbent and allow many dye molecules to bind to adsorbent surface. Previous researchers have reported similar uses of UAA in an aqueous adsorption experiment.[37,38]

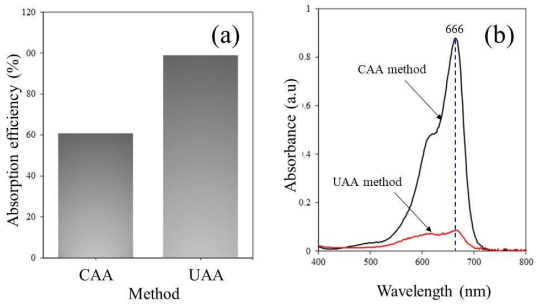

Fig.-6: (a) Adsorption Efficiency of MB from Solution using UAA Method and (b) CAA Method at 300 rpm (Condition of Both Methods were Similar, Otherwise Stated: Adsorbent Dosage = 2.5 g/L, Initial MB conc. = 20 ppm, Solution pH = 10, and Adsorption Time = 10 min)

The pH of the dye solution is crucial as it directly affects the charge of the adsorbent surface during the process of molecule adsorption. The upshot of pH on the adsorption efficiency of calcined OB-RHA SiO_2 for MB removal was investigated at pH 4, 7, and 10. As displayed in Fig.-7a, the lowest adsorption efficiency of 43.48% was found at a pH of 4 and then increased as the pH of solutions increased, yielding a maximum adsorption efficiency of 98.43% at a pH of 10. In general, the adsorption process in a solution involves surface chemistry and interaction between the adsorbate and the adsorbent, both of which are significantly influenced by the solution pH, which in turn affects the dye adsorption efficiency.[39,40] In a solution, when the concentration of -OH increases as the pH rises, the adsorbent surface develops a more negative charge, favoring binding more adsorbate cations. Hence, basic media is unquestionably favorable for removing cationic dyes. However, the opposite condition will occur in a lower pH solution with acidic properties and a lower -OH concentration. In more acidic solutions, the adsorbent surface develops a more positive charge and a proclivity to bind more anionic dyes.[40] This situation may be favorable in achieving high removal efficiency of anionic dyes. For these reasons, the adsorption of cationic dye MB in basic media (pH 10) is more advantageous than acidic media (pH 4) in terms of increasing the adsorption efficiency of calcined OB-RHA SiO_2. Kuang *et al.* [41] and Naseri *et al.*[42] observed a similar finding involving

the effect of pH on MB adsorption from solution using surfactant-modified activated carbon and titania-based nano adsorbent, respectively. The initial concentration of dye highly influences its interaction with the adsorbent surface and, in turn, will affect the adsorption efficiency.[40] The influence of the initial concentration of MB was evaluated by varying the initial MB concentration ranging from 10 to 40 ppm. As it can be seen in Fig.-7b, the lowest initial MB concentration (10 ppm) generates the highest adsorption efficiency, accounting for 99.64%, and continues to decrease up to 38.47% adsorption efficiency at 40 ppm of initial MB concentration. These findings imply fewer available dye molecules at low initial concentrations are less than the number of surface-active adsorbent sites. While at high concentrations, all active sites have been covered by dye molecules, resulting in MB molecules not being adsorbed completely at surface adsorbent.[39] Under the experimental conditions of this study, an initial MB concentration of 20 ppm with an adsorption efficiency of 98.83% is considered the endpoint of the adsorption process. According to Szende and Eszter, as cited in Rapo *et al*.,[40] the endpoint of an adsorption process is the point at which the volume of the solid adsorbent and dye solution reaches equilibrium stability.

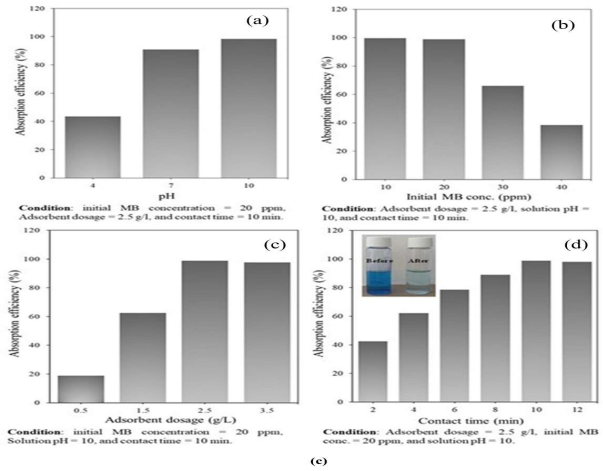

Fig.-7: (a) Dependency Pattern of MB Adsorption on the pH of the Solution, (b) Initial Concentration of MB, (c) the Adsorbent Dosage of Adsorbent, and (d) Adsorption Time (Inset Shows Color Change on MB Solution Before and After Adsorption)

The absorbent dosage is an essential factor to consider in achieving optimum efficiency in an adsorption process. To estimate the effect of adsorbent dosage, the mass of calcined OB-RHA SiO_2 was varied from 0 to 3.5 g/L and the results are portrayed in Fig.-7c. The adsorption efficiency of OB-RHA SiO_2 as adsorbents increases gradually from 42.36 to 98.85 % with increasing the dosage from 0.5 to 2.5 g/L and then tends to remain constant at the dosage of 3.5 g/L. The amount of adsorbate that can be adsorbed during an adsorption process is limited by the amount of adsorbent. This implies that the mechanism is dependent on the interaction between surface active site of the adsorbent and the adsorbate molecules.[39] In small adsorbent dosages, the number of surface-active sites available is insufficient to adsorb all adsorbate molecules in solution, resulting in low adsorption efficiency. With an increase in the dosage of the adsorbent, there is a corresponding rise in the amount of surface active sites that can absorb the adsorbate.[40] Another significant factor impacting adsorption efficiency is the time the adsorbate molecule diffuses from the solution to the adsorbent surface.[40] The effect of adsorption time was investigated by varying the contact time from 0 to 12 minutes. As presented in Fig.-7d, adsorption increases sharply from the first 2 min, resulting in 42.36% adsorption efficiency, and then gradually increases up to 10 min, generating an optimum adsorption efficiency of 98.83%. The results imply that longer contact time has a favorable effect on adsorption until a state of equilibrium is reached between the active sites of the adsorbent and the dye molecules.[39] Furthermore, the efficiency exhibits a near-constant value at 12 minutes due to the lack of substantial variation in the MB concentration in the solution. This indicates that, under the experimental conditions of this study, the adsorption equilibrium time is ten minutes. The inset of Fig.-7d displays the color changes of MB solution (20 ppm, pH 10) from blue to a clear solution after 10 min of adsorption using calcined OB-RHA SiO_2 (2.5 g/L).

CONCLUSION

The present study employed a simple digestive technique involving leaching and precipitation processes on a laboratory scale to fabricate SiO_2 from OB-RHA. The characterization results indicate that the calcined OB-RHA SiO_2 exhibited an amorphous microsphere structure with moderate aggregation and the presence of methanol during extraction process plays a vital role on the formation of such a spherical particle shape. The utilization of the UAA method has enhanced higher efficiency in MB removal than the CAA method. Enhanced adsorption efficiency was obtained as the solution pH was increased but the efficiency declined when both adsorbate concentration and adsorbent dosage were exceeded beyond the optimal levels. Conclusively, amorphous OB-RHA SiO_2 could be proposed as a viable and promising adsorbent in an ultrasound-assisted adsorption process for dye removal from solution. However, before amorphous OB-RHA SiO_2 can be used to treat dye waste at an industrial scale, an optimization study to relate multiple parameters of the adsorption process results in the most optimal values for those factors is highly required.

ACKNOWLEDGMENTS

The authors extend their sincere gratitude to RCC-BRIN for providing the necessary laboratory facilities and infrastructure to enable the execution of this study. The financial support from the Indonesian Government work through the Nanotechnology and Advanced Materials Programs, namely the Nanotechnology and Materials Research Organization-BRIN (No, 3/III.10/HK/2023) is thankfulness. E-Layanan Sains (ELSA)-BRIN was also acknowledged by the authors for granting access to the necessary material characterization resources for this investigation.

CONFLICT OF INTERESTS

The authors hereby affirm that they have no conflicts of interest to disclose.

AUTHOR CONTRIBUTIONS

All the authors contributed significantly to this manuscript, participated in reviewing/editing and approved the final draft for publication. The research profile of the authors can be verified from their ORCID ids, given below:

Q. Lailiyah http://orcid.org/0000-0002-9918-1272
N. T. E. Darmayanti http://orcid.org/0000-0003-0461-3712
M.R. Mulyana http://orcid.org/0009-0002-5492-0016
N. Nuryatini http://orcid.org/0009-0002-1301-9854
A. Hapiddin http://orcid.org/0000-0001-6579-6423
B. Basuki http://orcid.org/0000-0002-7435-1714
O. Zuas http://orcid.org/0000-0002-0101-5277
S. A. Rahmah http://orcid.org/0009-0007-0893-3074
A. N. Fadhila http://orcid.org/0009-0000-1905-8278
N. Aryana http://orcid.org/0009-0004-8250-1040
H. H. Kurniawan http://orcid.org/0000-0002-6863-1947
A. Andreas http://orcid.org/0009-0002-4344-6363
W. K. Restu http://orcid.org/0000-0002-7536-3610
F. Aulia http://orcid.org/0000-0002-2203-6050
T. Sudiro http://orcid.org/0000-0001-7872-914X
D. Nanto http://orcid.org/0000-0003-1148-6053

REFERENCES

1. H. B. Dizaji, T. Zeng, I. Hartmann, D. Enke, T. Schliermann, V. Lenz, and M. Bidabadi, *Applied Science,* **9(6)**, 1083(2019), https://doi.org/10.3390/app9061083
2. A. Daulay, Andriyani, Marpongahtun, and S. Gea, *Rasayan Journal of Chemistry*, **14(3)**, 2125(2021), http://doi.org/10.31788/RJC.2021.1436351
3. S. Aprilia, C.M. Rosnelly, Zuhra, F. Fitriani, E. H. Akbar, M. Raqib, K. Rahmah, A. Amin, and R.A. Baity, *Materals Today: Proceeding,* **87(2)**, 225(2023), https://doi.org/10.1016/j.matpr.2023.02.403
4. M. El-Sakhawy, A.M. Adel, M.A. Diab, and M. Al-Shemy, *Biomass Conversion and Biorefinery*, **12,** 4709(2022), https://doi.org/10.1007/s13399-020-01112-2
5. M.D. Villota-Enríquez, and J.E. Rodríguez-Páez, *Materials Chemistry and Physics*, **301**, 127671(2023), https://doi.org/10.1016/j.matchemphys.2023.127671
6. G. Smagulova, A. Imash, A. Baltabay, B. Kaidar, and Z. Mansurov, *C*, **8(4)**, 55(2022), https://doi.org/10.3390/c8040055
7. M. Laad, In Proceedings of the International Conference on Energy, Communication, Data Analytics and Soft Computing, Chennai, India, pp. 1946-1952 (2017), https://10.1109/ICECDS.2017.8389790
8. M.S.C. Rao, S. Packialakshmi, B. Rath, S.A. Alharbi, S. Alfarraj, and T R. Praveenkuma, B. Gavurová, *Environmental Research*, **231**, 116010(2023), https://doi.org/10.1016/j.envres.2023.116010
9. R. Sekifuji, and M. Tateda, *Sustainable Environmental Research*, **29**, 11(2019), https://doi.org/10.1186/s42834-019-0011-x
10. J.B. Haider, M.I. Haque, M. Hoque, M.M. Hossen, M. Mottakin, M.A. Khaleque, M.A.H. Johir, J.L. Zhou, M.B. Ahmed, and M. Zargar, *Journal of Cleaner Production*, **380**, 135121(2022), https://doi.org/10.1016/j.jclepro.2022.135121
11. N.T. Nguyen, S.-S. Chen, N.C. Nguyen, H.T. Nguyen, H.H. Tsai, and C.T. Chang, *Journal of Nanoscience and Nanotechnology,* **16(4)**, 4108(2016), https://doi.org/10.1166/jnn.2016.10704
12. E.C. Peres, N. Favarin, J. Slaviero, A.R.F. Almeida, M.P. Enders, E.I. Muller, and G.L. Dotto, *Materials Letters*, **231**, 72(2018), https://doi.org/10.1016/j.matlet.2018.08.018
13. H.T. Thu, L.T. Dat, and V.A. Tuan, *Vietnam Journal of Chemistry,* **57(2)**, 175(2019), https://doi.org/10.1002/vjch.201900012
14. G.M.K. Tolba, N.A.M. Barakat, A.M. Bastaweesy, E.A. Ashour, W. Abdelmoez, M.H. El-Newehy, S.S. Al-Deyab, and H.Y. Kim, *Journal of Industrial and Engineering Chemistry*, **29**, 134(2015), https://doi.org/10.1016/j.jiec.2015.03.025
15. J.A.S. Costa and C.M. Paranhos, *Journal of Cleaner Production,* **192**, 688(2018), https://doi.org/10.1016/j.jclepro.2018.05.028
16. H. Revathi, A. Xavier, M.D. Kumar, T. Saranya, A. Kaviyarasu, and T. Murugan, *Rasayan Journal of Chemistry,* **12(2)**, 719(2019), https://dx.doi.org/10.31788/RJC.2019.1225094
17. Y.S. Wong, W.H. Kwan, and M. Lim, *AIP Conference Proceedings*, **2157**, 020027(2019), https://doi.org/10.1063/1.5126562
18. H.H. Ali, H.H. Mihsen, and K.A. Hussain, *BioNanoScience*, **13**, 1163(2023), https://doi.org/10.1007/s12668-023-01144-8
19. V.-C. Niculescu, and M.S. Raboaca, *Catalysts*, **11(7)**, 815(2021), https://doi.org/10.3390/catal11070815
20. S.A. Ajeel, K.A. Sukkar, and N. K. Zedin, *Engineering and Technology Journal*, **39(1A)**, 56(2021), https://doi.org/10.30684/etj.v39i1A.1696
21. S. Azat, A.V. Korobeinyk, K. Moustakas, and V.J. Inglezakis, *Journal of Cleaner Production,* **217**, 352(2019), https://doi.org/10.1016/j.jclepro.2019.01.142
22. L. A. Q. Sierra, and D.M.E. Sierra, *The Journal of the Minerals*, **71**, 302(2019), https://doi.org/10.1007/s11837-018-3199-z
23. G. Spiekermann, M. Steele-MacInnis, C. Schmidt, and S. Jahn, *The Journal of Chemical Physics,* **136(15)**, 154501(2012), https://doi.org/10.1063/1.3703667
24. H. Kang, *IOP Conference Series: Earth and Environmental Science*, **726**, 012001(2020), https://doi.org/10.1088/1755-1315/726/1/012001

25. X. Yuan, and A.N. Cormack, *Journal of Non-Crystalline Solids*, **319(1-2)**, 31(2003), https://doi.org/10.1016/S0022-3093(02)01960-9
26. P. McMillan, *American Mineralogist*, **69(7-8)**, 622(1984)
27. M. A. Pereira, J. E. de Oliveira, and C.S. Fonseca, *Cerâmica*, **67(383)**, 333(2021), https://doi.org/10.1590/0366-69132021673833134
28. J.C. Mikkelsen Jr., and F.L. Galeener, *Journal of Non-Crystalline Solids*, **37(1)**, 71(1980), https://doi.org/10.1016/0022-3093(80)90480-9
29. I. N. Chakraborty, and R.A. Condrate, *Physics and Chemistry of Glasse*s, **26**, 68(1985).
30. W. Trisunaryanti , Triyono, C. Paramesti, S. Larasati, N. R. Santoso, and D.A. Fatmawati, *Rasayan Journal of Chemistry*, **13(3)**, 1386(2020), https://dx.doi.org/10.31788/RJC.2020.1335840
31. P.G. Li, M. Lei, and W.H. Tang, *Materials Letters,* **64(2)**, 161(2010), https://doi.org/10.1016/j.matlet.2009.10.032
32. M. Thommes, K. Kaneko, A.V. Neimark, J.P. Olivier, F. Rodriguez-Reinoso, J. Rouquerol, and K.S.W. Sing, *Pure and Applied Chemistry,* **87(9-10)**, 1051(2015), https://doi.org/10.1515/pac-2014-1117
33. I.J. Fernandes, D. Calheiro, A.G. Kieling, C.A.M. Moraes, T.L.A.C. Rocha, F.A. Brehm, and R.C.E. Modolo, *Fuel*, **165**, 351(2016), https://doi.org/10.1016/j.fuel.2015.10.086
34. J.Y. Park, Y.M. Gu, S.Y. Park, E.T. Hwang, B.-I. Sang, J. Chun, and J.H. Lee, *Sustainability*, **13(13)**, 7350(2021), https://doi.org/10.3390/su13137350
35. T.N.M. Bernards, M.J. van Bommel, and A.H. Boonstra, *Journal of Non-Crystalline Solids*, **134(1-2)**, 1(1991), https://doi.org/10.1016/0022-3093(91)90005-Q
36. A.M. Ealias and M.P. Saravanakumar, *Critical Reviews in Environmental Science and Technology,* **49(21)**, 1959(2019), https://doi.org/10.1080/10643389.2019.1601488
37. A. Assafi, Y.A.E.H. Ali, R.S. Almufarij, L. Hejji, N. Raza, L.P. Villarejo, B. Souhail, A. Azzouz, and E.A. Abdelrahman, *Heliyon,* **9(11),** e22001(2023), https://doi.org/10.1016/j.heliyon.2023.e22001
38. M. Amin, P. Chetpattananondh, and M.N. Khan, *Journal of Environmental Chemical Engineering*, **8(6)**, 104403(2020), https://doi.org/10.1016/j.jece.2020.104403
39. S. Dutta, B. Gupta, S.K. Srivastava, and A.K. Gupta, *Materials Advances*, **2(14)** , 4497(2021), https://doi.org/10.1039/D1MA00354B
40. E. Rápó and S. Tonk, *Molecules*, **26(17)**, 5419(2021), https://doi.org/10.3390/molecules26175419
41. Y. Kuang, X. Zhang, and S. Zhou, *Water*, **12(2)**, 587(2020), https://doi.org/10.3390/w12020587
42. K. Naseri, and A. Allahverdi, *Research on Chemical Intermediates*, **45**, 4863(2019), https://doi.org/10.1007/s11164-019-03866-5

[RJC- 8726/2023]